INTERNATIONAL JOURNAL FOR NUMERICAL METHODS IN FLUIDS, VOL. 9, 963–985 (1989)

SECOND-MOMENT CLOSURE AND ITS USE IN MODELLING TURBULENT INDUSTRIAL FLOWS

B. E. LAUNDER

Department of Mechanical Engineering, University of Manchester, Institute of Science and Technology, PO Box 88, Manchester, U.K.

SUMMARY

Second-moment turbulence models focus directly on the transport equations for the Reynolds stresses rather than supposing the stress and strain fields to be directly linked via an eddy viscosity. This elaboration enables the effects of complex strains and force fields on the turbulence structure to be better captured. The paper summarizes the principal modelling strategies adopted for the unknown processes in these equations and presents the forms that have been found most useful in engineering calculations. Methods adopted for overcoming significant problems of numerical instability and lack of convergence compared with eddy-viscosity-based schemes are also presented. Applications involving momentum and heat transfer in complex flows are drawn from the advanced technology sectors of the power generation and aircraft industries.

KEY WORDS Second moment Turbulence Transport equations Reynolds stress Complex flows Industrial applications

INTRODUCTION

The past decade has seen major extensions in the range of turbulent flows that can feasibly be resolved by a numerical solution of the Reynolds equations. Complex three-dimensional and recirculating flows directly relevant to industrial situations now fall within the scope of computer simulation. One outcome of this is the increasing use of commercially developed flow simulation software, often by persons with no detailed familiarity with computational fluid dynamics. These developments might give the impression that the CFD of turbulent flows is now a mature technology with relatively minor advances remaining to be made. Such an impression would, however, be very wide of the mark.

At present the great majority of industrial flow computations are based on an eddy (or turbulent) viscosity representation of the Reynolds stresses, the most extensively used version[1] being one where the turbulent viscosity at a point is obtained from local values of the turbulent kinetic energy k and its rate of dissipation ε, which in turn are obtained from transport equations solved simultaneously with those for the mean velocity components. It is, however, well established that eddy viscosity models do not correctly mimic the sensitivity of the turbulent stresses to streamline curvature and body forces or to situations where transport effects are large. The present paper is therefore concerned with the use of a different approach to determining the turbulent stresses: second-moment closure. With models of this type one obtains, by taking velocity-weighted moments of the Navier–Stokes equations, a set of exact equations for the transport of the Reynolds stresses themselves. The equations are unclosed, however, so the task of the turbulence model is to devise approximations for the unknown turbulence correlations in

0271-2091/89/080963-23$11.50 *Received 8 December 1987*

terms of known or determinable quantities. Models of this type are, in principle, free from the objections noted above to eddy viscosity models. The first such scheme was put forward by Rotta,[2] though it was not until the late 1960s and early 1970s that one began to see (e.g. 3–6) significant use of such models and then only for two-dimensional thin shear flow computations. For such cases the solution proceeds in a marching manner with the flow streamlines well aligned with the grid lines.

From a numerical point of view, use of a second-moment closure greatly complicates the task of solution compared with that when an eddy viscosity scheme is adopted. This is especially the case in situations where, due to flow recirculation, a fully iterative solution must be adopted over the flow domain. While the first application of this type of model to a recirculating flow appeared in 1976,[7] it is now acknowledged that the results were very severely contaminated by numerical diffusion. The more extensive use of second-moment closures in complex flows has thus had to await the invention of stable yet non-dispersive practices for discretizing convective transport; the development of stability-promoting practices in handling the Reynolds stresses; and, not least, the increase of computational power that allows *routine* computations of such flows to be made.

The present contribution summarizes briefly the more widely adopted modelling practices in second-moment closure and the special numerical practices that can help convergence. Applications drawn from the work of the CFD group at UMIST convey an impression of the capabilities of the present generation of second-moment closures in modelling complex flows.

MATHEMATICAL REPRESENTATION

Framework for second-moment closure

We write the Navier–Stokes equations for a fluid in turbulent motion as

$$\frac{\partial \tilde{\rho}\tilde{U}_i}{\partial t}+\frac{\partial}{\partial x_k}\tilde{\rho}\tilde{U}_k\tilde{U}_i=-\frac{\partial \tilde{P}}{\partial x_i}+\tilde{F}_i+\frac{\partial}{\partial x_k}\left(\mu\left(\frac{\partial \tilde{U}_i}{\partial x_k}+\frac{\partial \tilde{U}_k}{\partial x_i}\right)-\frac{2}{3}\mu\delta_{ik}\frac{\partial \tilde{U}_m}{\partial x_m}\right) \tag{1}$$

where U_i denotes velocity in direction x_i, ρ the density, P the pressure and F_i an effective body force (due perhaps to buoyancy or rotation of the co-ordinate frame). The tilde superscript indicates 'instantaneous value of', which comprises a mean and turbulent part. Thus $\tilde{U}_i \equiv U_i + u_i$, where in general upper case letters (with no superscript) denote mean values and lower case letters turbulent quantities. The mean value of velocity U_i is obtained by applying the following operation to $\tilde{U}_i$:

$$U_i=\frac{1}{2T}\int_{\lim T\to\infty}^{T}\tilde{U}_i\,\tilde{W}\,\mathrm{d}t, \tag{2}$$

where $\tilde{W}$ is some user-chosen weighting function for which $(1/2T)\int_{-T}^{T}\tilde{W}\,\mathrm{d}t = 1$.

In analysing turbulent flows involving combustion, where large variations of density occur, $\tilde{W}$ is often chosen as $\tilde{\rho}/\rho$, e.g. Reference 8. Other forms of weighting or 'conditioning' functions are sometimes used in analysing intermittently turbulent flows. For the discussion in the present paper, however, the weighting function is taken identically equal to unity. Moreover, while mean density variations are admissible, it is assumed that turbulent fluctuations in density are unimportant except in the buoyancy force term $\tilde{F}_i$ (the so-called Boussinesq approximation). Under this restriction the averaging of each of the terms of equation (1) for a statistically stationary

flow produces the Reynolds equation

$$\frac{\partial}{\partial x_k}\rho U_k U_i = -\frac{\partial P}{\partial x_i} + \frac{\partial}{\partial x_k}\left[\mu\left(\frac{\partial U_i}{\partial x_k} + \frac{\partial U_k}{\partial x_i}\right) - \rho\,\overline{u_i u_k}\right], \tag{3}$$

where $\overline{u_i u_k}$ are the Reynolds stresses for whose determination a path must be provided (the overbar simply implies the averaging of the product $\overline{u_i u_k}$ as indicated in (2) with $\tilde{W} \equiv 1$).

In second-moment closure the first step is to obtain a set of transport equations for these stress components. Such a set may be obtained by multiplying (1) by u_j and averaging and then adding to it the same equation but with the subscripts i and j interchanged. After a certain amount of manipulation and taking note that the fluctuating velocity field is incompressible, i.e. $\partial u_i/\partial x_i = 0$, we obtain the following equation describing the rate of change of $\overline{u_i u_j}$:

$$\begin{aligned}
\underbrace{\frac{\partial}{\partial x_k}(\rho U_k \overline{u_i u_j})}_{C_{ij}} = & -\rho\left(\overline{u_j u_k}\frac{\partial U_i}{\partial x_k} + \overline{u_i u_k}\frac{\partial U_j}{\partial x_k}\right) && P_{ij}\\
& + (\overline{u_j f_i} + \overline{u_i f_j}) && F_{ij}\\
& + \overline{p\left(\frac{\partial u_i}{\partial x_j} + \frac{\partial u_j}{\partial x_i}\right)} && \phi_{ij}\\
& - \frac{\partial}{\partial x_k}\left(\rho\,\overline{u_i u_j u_k} + \overline{p u_i}\,\delta_k + \overline{p u_j}\,\delta_{ik} - \mu\frac{\partial \overline{u_i u_j}}{\partial x_k}\right) && d_{ij}\\
& - 2\mu\,\overline{\frac{\partial u_i}{\partial x_k}\frac{\partial u_j}{\partial x_k}} && \rho\,\varepsilon_{ij}.
\end{aligned} \tag{4}$$

The equation is arranged so that each distinct physical process contributing to the change of $\overline{u_i u_j}$ appears on a separate line. In the right-hand column a short-hand symbol is given which, for brevity, we shall normally adopt in referring to these processes. We notice that the direct effects of mean shear in this equation (P_{ij}) can be handled without approximation since the velocity and Reynolds stress fields are themselves the subject of conservation equations. The same is normally true of F_{ij}, though in the case of buoyancy F_{ij} contains fluctuating density–velocity products for which an additional set of equations must be supplied. Space limitations preclude their inclusion in the present contribution: the interested reader is referred to Reference 9.

The fact that major source terms in (4) are exactly determinable is the main reason to expect that closures formed at second-moment level will capture the behaviour of the turbulent stress field with greater fidelity than eddy viscosity models.

A simple closure of the Reynolds stress transport equation

Apart from the minor contribution from viscous diffusion of $\overline{u_i u_j}$, the remaining processes in (4) cannot be handled exactly at second-moment level and must be 'modelled'. The processes in question are those of diffusion (d_{ij}), viscous dissipation (ε_{ij}) and a non-diffusive pressure interaction, ϕ_{ij}, usually called the pressure–strain correlation. Surrogate forms devised to imitate the real processes will incorporate at least some of the formal characteristics of the tensors they replace: dimensional homogeneity; rank, symmetry and contraction properties of the original form; invariance to the co-ordinate frame adopted for monitoring the flow development. One may also wish to insist that the approximation should give exactly the correct results in certain limiting cases where the magnitude of the original correlation is known (e.g. in isotropic turbulence). These

formal constraints, however, need to be weighed against the benefits of simplicity (from both computational and conceptual viewpoints) and the inherent limitations of a second-moment closure which entirely disregards such features as intermittency. For those wishing to compute industrial flows, the interwoven principles of diminishing returns and receding influence should always be borne in mind. Despite what the literature may sometimes seem to suggest, turbulence modelling is in no danger of becoming just another branch of rational mechanics.

In the present subsection we present a very simple set of approximations that is the only form to have been widely used in computing complex industrial-type flows. It is this version that has been adopted in most of the applications in the next section.

Dissipation ε_{ij}. The conventional (albeit not unchallenged) view is that the very fine-grained eddies which are essential to account for the destruction of turbulence energy by viscous action are formed by a large number of interactions in which large eddies are successively broken down into finer-scale motions. As this breakdown proceeds, the strong directional orientation imprinted on the larger eddies by the mean strain field gradually gets lost so that, by the time the scales are small enough for significant kinetic energy to be dissipated (implying an eddy Reynolds number of around unity), the motions are *isotropic*. In this event we can replace ε_{ij} by

$$\varepsilon_{ij} = \tfrac{2}{3}\delta_{ij}\varepsilon, \tag{5}$$

where $\varepsilon \equiv \overline{\nu(\partial u_i/\partial x_k)^2}$ is the kinematic rate of dissipation of turbulence energy ($\nu \equiv \mu/\rho$).

The determination of ε itself is one of the weakest points in second-moment closure. Although an exact equation for this correlation can be obtained from the Navier–Stokes equations by similar steps to those producing (4),[10] the resultant equation does not in practice represent a useful starting point. The reason is that the quantities appearing in it all relate to interactions among the finest scales of motion present. Yet only in a legalistic sense is the rate of energy dissipation determined by these processes. The *real* controlling factor is the rate at which energy 'cascades' from large- to small-scale eddies. The interactions producing that transfer are larger-scale, essentially inviscid motions. Accordingly, in formulating a model equation for ε, one relies heavily on analogy, intuition and experiment. The form usually adopted may be written

$$\frac{\partial}{\partial x_k}\rho U_k\varepsilon = c_\varepsilon\frac{\partial}{\partial x_k}\left(\frac{\overline{u_k u_l}}{\varepsilon}k\frac{\partial\varepsilon}{\partial x_l}\right) + 0{\cdot}5\frac{\varepsilon}{k}(c_{\varepsilon 1}P_{kk} + c_{\varepsilon 3}F_{kk}) - c_{\varepsilon 2}\frac{\varepsilon^2}{k}. \tag{6}$$

The three terms on the right side of (6) are respectively diffusive, generative and dissipative in character. The diffusion process is modelled by the generalized gradient diffusion hypothesis of Daly and Harlow.[4] The value usually adopted for c_ε—about 0·18—is typical of those chosen when applying this submodel to other processes.

The forms of the generation and dissipation terms are directly analogous to those that appear in the turbulent kinetic energy equation (whose exact form is obtained by summing (4) with $i = j$ and dividing by two). There is no very good physical reason to suppose that the rate of transfer of turbulent kinetic energy from large to small eddies is so directly related to turbulent energy generation (indeed, some alternative proposals will be mentioned later), but it is the simplest possible assumption and often leads to satisfactory results. The resultant predictions are highly sensitive to the choice of $c_{\varepsilon 1}$ and $c_{\varepsilon 2}$: a change in either by 1% typically alters the computed rate of spread of a jet by 4%. What are usually regarded as 'standard' values are chosen by matching data for the decay of turbulence energy behind a grid and the rate of spread of a plane jet in stagnant surroundings. The diffusion coefficient c_ε, is then chosen to give a length scale variation for flow near a wall in local equilibrium consistent with the 'universal' semilogarithmic velocity profile.

One thus obtains

$$c_{\varepsilon 1} = 1{\cdot}44, \qquad c_{\varepsilon 2} = 1{\cdot}92, \qquad c_{\varepsilon} = 0{\cdot}18.$$

Logic suggests that $c_{\varepsilon 3}$ should be chosen equal to $c_{\varepsilon 1}$. While this choice is sometimes made, other (usually smaller) values are just as often chosen. It is an area where further work is needed.

Pressure–strain correlation. The pressure–strain correlation contains within it two types of process that require modelling separately. This may be clearly seen by forming a Poisson equation for the fluctuating pressure p (by taking the divergence of the Navier–Stokes equations and subtracting the mean part). On integrating that equation and multiplying each side by the instantaneous strain and averaging, one obtains for a homogeneous field away from the vicinity of rigid boundaries[11] where body forces are negligible

$$\phi_{ij} = \frac{1}{4\pi} \int \left[\overline{\left(\frac{\partial^2 u_l u_m}{\partial x_i \partial x_m} \right)' \left(\frac{\partial u_i}{\partial x_j} + \frac{\partial u_j}{\partial x_i} \right)} + 2 \left(\frac{\partial U_l}{\partial x_l} \right) \overline{\left(\frac{\partial u_m}{\partial x_l} \right)' \left(\frac{\partial u_i}{\partial x_j} + \frac{\partial u_j}{\partial x_i} \right)'} \right] \frac{\mathrm{d\ Vol}}{\underline{r}}, \tag{7}$$

where the primed quantities are evaluated at a distance $\underline{r}$ from the point in question and the integration extends over all space (though in practice the contribution is limited to distances from the point comparable with the turbulent macroscale). Thus the first integral in (7) contains only turbulent velocities (ϕ_{ij1}), while the second (ϕ_{ij2}) comprises linear mean-strain elements multiplying double velocity products. The two contributions are here referred to as the 'turbulence' and 'mean-strain' parts of ϕ_{ij}. The latter is also known as the 'rapid' term because some workers have used results from rapid distortion theory to model this process. From there, however, verbal simplification has reduced 'rapid' to 'fast' with the foreseeable result that the 'turbulence' part is now often called the 'slow' term. So much for the etymology.

Considerable efforts are now being made in devising widely valid models of ϕ_{ij1} and ϕ_{ij2}, work that springs principally from pioneering efforts of Lumley.[12] The industrial flow computations presented in the next section have so far mainly adopted the simpler intuitive versions noted below which are only loosely connected with the two integrals in (7). One of the most enduring models in second-moment closure is Rotta's[2] linear return-to-isotropy model of ϕ_{ij1}:

$$\phi_{ij1} = -c_1 \rho \varepsilon a_{ij}, \tag{8}$$

where a_{ij} is the dimensionless stress anisotropy tensor $(\overline{u_i u_j} - \frac{1}{3}\delta_{ij}\ \overline{u_k u_k})/k$. For decaying anisotropic turbulence, with ε_{ij} represented by (5), the above model actually causes a tendency towards isotropy only if c_1 is greater than unity. If a constant value is to be chosen for this coefficient, the best choice seems to be close to 2·0.

The best simple model for the mean-strain part of ϕ_{ij} is known as the isotropization of production (IP) model:[13]

$$\phi_{ij2} = -c_2(P_{ij} - \tfrac{1}{3}\delta_{ij}P_{kk}). \tag{9}$$

Its form is directly analogous to (8). If ϕ_{ij} is regarded as turbulence's taxation system, ϕ_{ij1} is a wealth tax while ϕ_{ij2} is an income tax—albeit with effectively negative taxation rates for members with less than the average wealth or income.

Figure 1 shows the range of values selected for c_1 and c_2 by different workers: there is evidently a vast range, but it is clear that all choices of c_1 and c_2 cluster close to the line $(1-c_2)/c_1 = 0{\cdot}23$. This is because for a simple shear flow in local equilibrium (i.e. where $\frac{1}{2}P_{kk} = \varepsilon$) the relative stress levels are uniquely a function of $(1-c_2)/c_1$. The entries for $c_2 = 0$ are proposals which entirely neglected the ϕ_{ij2} process, while the original proposal of Naot *et al*,[13] who proposed the largest value of c_2,

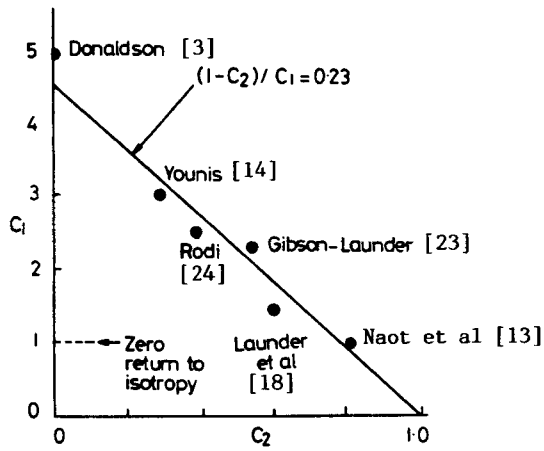

Figure 1. c_1–c_2 map

did not explicitly include a contribution from ϕ_{ij1} (though these workers also assumed $\varepsilon_{ij}=(u_iu_j/k)\varepsilon$—which is equivalent to choosing $c_1=1$ if (5) is adopted for ε_{ij}). In suddenly distorted isotropic turbulence one may show that $c_2=0{\cdot}6$ exactly and it is this marker that has generally led workers to opt for values of c_2 in this region. A recent exception to this consensus is the recommendation of Younis[14]—$c_2=0{\cdot}3$, $c_1=3{\cdot}0$—a choice which gives more weight to the turbulence than the mean-strain part of ϕ_{ij}. This choice arose from the discovery that swirling flows were captured much better with this combination.[15]

There is, however, a good reason for not expecting (9), as it stands, to do well in predicting swirling flows. It is that P_{ij} is not an objective tensor: its form depends on the reference frame of the observer. One might, for example, study the development of an axisymmetric swirling flow either in stationary cylindrical polar co-ordinates or in a frame that rotates about the symmetry axis. In that event P_{ij} will depend on the rate of rotation of the axis. Of course in a non-inertial frame a co-ordinate rotation source F_{ij} enters the equations but the sum of P_{ij} and F_{ij} is also dependent on the rotation rate. Only if we bring to this group the convective transport tensor C_{ij} from the left side of (2) do we arrive at a materially indifferent form. This consideration suggests that in place of P_{ij} one should really adopt $P_{ij}+F_{ij}-C_{ij}$ in (9), i.e.

$$\phi_{ij2}=-c_2[P_{ij}+F_{ij}-C_{ij}-\tfrac{1}{3}\delta_{ij}(P_{kk}-C_{kk})], \tag{10}$$

since F_{kk} is zero. In a stationary reference frame in local equilibrium the original form is recovered. In fact our experience at UMIST suggests that $C_{ij}-\frac{1}{3}\delta_{ij}C_{kk}$ makes a negligible contribution except in swirling flows.

Another widely used, interesting but not recommended version of ϕ_{ij2} is the more elaborate quasi-isotropic (QI) model:[16,17]

$$-\left(\frac{\gamma+8}{11}\right)(P_{ij}-\tfrac{1}{3}\delta_{ij}P_{kk})-\left(\frac{30\gamma-2}{55}\right)k\left(\frac{\partial U_i}{\partial x_j}+\frac{\partial U_j}{\partial x_i}\right)-\left(\frac{8\gamma-2}{11}\right)(D_{ij}-\tfrac{1}{3}\delta_{ij}D_{kk}), \tag{11}$$

where

$$D_{ij}\equiv-\left(\overline{u_iu_k}\frac{\partial U_k}{\partial x_j}+\overline{u_ju_k}\frac{\partial U_k}{\partial x_i}\right).$$

The formula has been obtained in many different ways by various groups. The simplest way is to assume that ϕ_{ij2} is expressible in terms of the most general sum of linear products of Reynolds stress and mean-strain elements. All but one of the coefficients are then fixed by applying symmetry, continuity and other consistency constraints; details are given in References 18–20. The QI model with $\gamma = 0{\cdot}4$ achieves reasonable success in thin shear flows but gives spectacularly bad results in swirling flows.[21] Current research suggests that the problem with (11) is not that the formal consistency analysis is inappropriate to turbulence modelling but rather that the basic form adopted for the analysis is insufficiently general.

Wall effects on the pressure–strain correlation ϕ_{ij}^{w}. The integral expression for ϕ_{ij} in (7) is complete only for flow regions uninfluenced by rigid boundaries. Walls, and indeed density interfaces in fluids generally, reflect pressure fluctuations, thus interfering with the normal redistributive actions of the pressure–strain correlation. This 'echo' effect is accommodated by the inclusion of terms whose strength depends on the ratio of the local turbulent length scale to the distance from the wall, x_n, i.e. $k^{3/2}/\varepsilon x_n$. Most workers have adopted simply a linear function of this parameter, though Naot and Rodi[22] found better agreement in their study of duct flows by using $(k^{3/2}/\varepsilon x_n)^2$. This has the effect of making the wall echo effect die off more rapidly. The usually adopted form for the complete wall reflection term is[23]

$$\phi_{ij}^{w} = [c_1'(\overline{u_k u_k}\, n_k n_m \delta_{ij} - \tfrac{3}{2}\overline{u_k u_i}\, n_k n_j - \tfrac{3}{2}\overline{u_k u_j}\, n_k n_i + c_2'(\phi_{km2}\, n_k n_m \delta_{ij} - \tfrac{3}{2}\phi_{ik2}\, n_k n_j - \tfrac{3}{2}\phi_{jk2}\, n_k n_i)]\left(\frac{k^{3/2}}{\varepsilon x_n}\right)^a, \tag{12}$$

where n_i is the unit vector normal to the wall and, as noted above, the exponent 'a' is taken as 1 or 2. Equation (12) should be regarded simply as an empirical fit to the observed effects of the wall. In fact, with this form it is not entirely possible to mimic the changes that the wall provokes. For example, in a simple shear flow (12) redirects a fraction of the energy earmarked for the direction normal to the wall equally to the two components parallel to the surface. Experiment suggests, however, that virtually all the energy that the normal fluctuations lose ends up in the streamwise component. Nevertheless, (12) has proved an adequate model in many cases. If one is dealing with flow in a plane channel, one finds a contribution from the two opposite walls; in a square channel all four sides make a contribution. The separate effects of each wall can be superimposed linearly. There is at present no scheme available for handling complex boundary topography such as grooved or ridged surfaces. While this is certainly a handicap in studying passive devices for near-wall flow management (e.g. for drag reduction or heat transfer enhancement), the latest models of ϕ_{ij} now emerging carry much of the echo effect in the wall boundary condition; accordingly, the importance of an explicit wall correction process, such as (11), is reduced.

Diffusion d_{ij}. The Daly–Harlow[4] generalized gradient diffusion hypothesis was mentioned in connection with the diffusion of ε. It is also the model usually adopted for modelling stress diffusion, i.e.

$$d_{ij} = c_s \frac{\partial}{\partial x_k}\left(\frac{k}{\varepsilon}\overline{u_k u_l}\frac{\partial \overline{u_i u_j}}{\partial x_l}\right), \tag{13}$$

the constant diffusion coefficient c_s taking a value of approximately 0·22. Although originally advanced as a model of the part of d_{ij} involving triple velocity products (cf (4)), it should be regarded as a composite model for both pressure- and velocity-driven diffusion. (As a model of just

the triple velocity product, the kernel of the $\partial/\partial x_k$ operator in (13), unlike $\overline{u_i u_j u_k}$, is not indifferent to the sequencing of the i, j, k indices.)

Equation (13) is not a particularly accurate model of d_{ij} but is relatively simple and is usually good enough for the purposes in question, diffusive transport being decidedly less crucial in the Reynolds stress budget than either ϕ_{ij} or ε_{ij}. It is not just that there are many flows where d_{ij} is very small; even where it is substantial, because the term acts as a spatial *redistributor* of $\overline{u_i u_j}$ rather than as a source or sink, it tends to have a relatively small effect on the rates of spread of a shear flow.

While there are exceptional cases—particularly where interfaces develop in a turbulent field—where modelling stress diffusion is quite critical, second-moment closure for industrial flows has often adopted simpler rather than more elaborate representatives of d_{ij}. The widely used algebraic second-moment (ASM) approach approximates both diffusive and convective transport in terms of the corresponding transports of k, the turbulence energy. The version proposed by Rodi[24] is the one often adopted:

$$C_{ij} = \frac{\overline{u_i u_j}}{k} C_k, \qquad d_{ij} = \frac{\overline{u_i u_j}}{k} d_k, \tag{14}$$

where C_k and d_k denote the convective transport rates of turbulent kinetic energy. A generalized version of (14)[25] has also been used which seems to give a somewhat better approximation of C_{ij} and d_{ij} at the cost of some sacrifice of simplicity and numerical stability. The major simplification that results from making such an approximation is that differentials of $\overline{u_i u_j}$ are entirely eliminated from the resultant closed form of (4). Thus one arrives at a set of *algebraic* rather than differential equations for the stresses. For example, if the approximations contained in equations (5), (8), (9) and (14) are introduced, one arrives at the following form:

$$a_{ij} \equiv \frac{\overline{u_i u_j} - \frac{1}{3}\delta_{ij}\overline{u_k u_k}}{k} = \frac{1 - c_2}{c_1 - 1 + \frac{1}{2}P_{kk}/\varepsilon} \frac{P_{ij} - \frac{1}{3}\delta_{ij}P_{kk}}{\varepsilon}. \tag{15}$$

Thus turbulent transport equations are required only for the evolution of k and ε.

While examples of ASM approaches will be given in the next section, in the writer's group (and also in several other groups in the UK) they are now being replaced by *differential* schemes. The problem with (14), or any of the alternatives, is that C_{ij}, which (as discussed above) is not an objective tensor, is being approximated by a form that *is*. Fu *et al.*[26] have reported the very serious differences that arise between differential and algebraic representations of transport in swirling flows. These have forced us to abandon the use of ASM schemes in these flows despite the advantage of computational economy that they bring.

Remarks on the numerical solution with second-moment closures

Our experience at UMIST is that there are so many differences in solution strategy required between including a second-moment closure and an eddy viscosity model into a 3D or elliptic 2D solver that one invariably produces two different computer programs rather than one code with different subroutines. Most aspects of our finite volume solution methodology with second-moment closures have been extensively considered by Huang and Leschziner[27] and Leschziner.[28] Here, therefore, only brief remarks are provided.

We note first that if one adopts the usual staggered velocity/pressure node cluster, numerical stability is increased and the amount of interpolation required decreased if the stresses are also staggered as shown in Figure 2.[7] The normal stresses are located at the scalar (pressure) node while the off-diagonal components are positioned so that they lie on the boundaries of the control

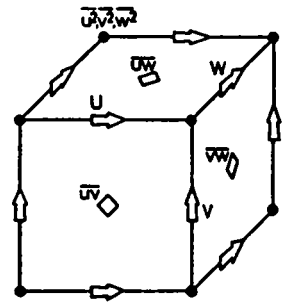

Figure 2. Staggered node cluster for Reynolds stresses and velocity

volumes of the velocity components in whose conservation equation they appear. Note that $\overline{uv}$ appears in the conservation equations for both U and V and is located at the appropriate intersection of the U and V control volumes.

In a three-dimensional flow we will find each stress component appearing in the budget equations for many of the other components. This very strong intercoupling suggests that one should opt for a simultaneous solution of the six components at a point. However, such a direct approach is spectacularly unstable partly, perhaps, because the stresses are scattered. The strategy evolved in Reference 27 is first to solve for the three coincident normal stresses, interpolating as necessary 'old' values of the shear stresses. When updated values of the normal stresses have been obtained at all nodes, the off-diagonal components are obtained by a pointwise substitution.[29]

An alternative grid layout is under evaluation at UMIST to allow *all* the stresses to be handled in the same way; we refer to it as the 'semi-staggered mesh' and it is illustrated in Figure 3: in a three-dimensional flow there are just two locations for dependent variables instead of seven for the usual scheme shown in Figure 2. The velocity components are all stored at the same location, which is offset from the scalar node at which pressure, energy dissipation rate and all the Reynolds stress components are calculated. If one needs to solve the thermal energy equation, this variable is also evaluated at the scalar node, while the turbulent heat fluxes are evaluated at the velocity nodes. This layout appears to offer a number of advantages over that of Figure 2, though there are also drawbacks, notably the larger number of velocity nodes that appear when the continuity equation is formulated.

The above discussion has concerned the *spatial* staggering of stress components relative to the velocity field. We note in passing that in time-dependent flows it has been found advantageous to stagger the stresses in time as well as space with respect to the velocity field.[30]

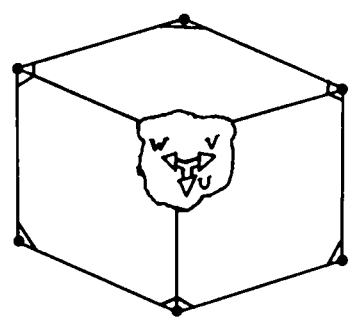

Figure 3. Semi-staggered mesh

Special measures also need to be adopted in the momentum equations when a second-moment closure is employed. With an eddy viscosity turbulence model there are strong diffusive connections with adjacent nodes and this feature is helpful in maintaining stability. The straightforward approach with a second-moment closure would be to incorporate the forces due to the Reynolds stresses acting on the control volume faces as sources and sinks. That approach, however, is highly unstable owing to the stiffness of the resultant equation set. One needs to build back into the difference equations something of the strong internodal coupling that is present in eddy viscosity schemes. Now, in the U_i momentum equation the Reynolds stress contribution is $-\partial\rho\,\overline{u_iu_j}/\partial x_j$. With an ASM approach the algebraic formula linking the stresses and strains will contain a term involving $\partial U_i/\partial x_j$. One may then designate the coefficient of that strain component as a pseudo-viscosity, $\tilde{\mu}_{ij}$ say (in general there will be three such terms in each of the U_i equations corresponding to the three x_j co-ordinate directions). Such terms are inserted in the solver as viscous-like contributions, i.e. the mean velocities in them are handled implicitly, while the remaining elements of the ASM formula are handled as explicit sources.

A differential stress model does not of course contain, at the level of the continuum transport equation for $\overline{u_iu_j}$, any part interpretable as a pseudo-viscosity (because the equation describes *rates of change* rather than prevailing levels of $\overline{u_iu_j}$). Nevertheless, once one forms the *difference* equations for $\overline{u_iu_j}$ there will be terms directly analogous to those appearing in the ASM that can be removed and treated in the solver via an effective diffusive coefficient. Of course $\tilde{\mu}_{ij}$ will be non-isotropic and will usually not exhibit symmetry in i and j,* but this feature brings no added problems.

Boundary conditions

While the application of boundary conditions with second-moment closures is not appreciably different from the practices for an eddy viscosity scheme, it is often a sufficiently vexing task for some brief remarks to be in order.

Plane or axis of symmetry. This is the simplest case. Axial velocity, ε and normal stress components approach the axis with zero gradient, while radial and circumferential velocities and shear stresses vanish.

Free surface (e.g. at a water/air interface). This is often incorrectly treated as a plane of symmetry. The normal stress perpendicular to the free surface vanishes. The appropriate boundary condition for ε is not entirely resolved: $\partial\varepsilon/\partial y$ provides a neutral constraint that exerts little effect away from the immediate vicinity of the surface. Far more important than boundary conditions is the inclusion of the 'echo' effect $\phi_{ij}^{w\,23}$ (see earlier).

Entraining boundary. This involves prescribed levels of the turbulent stresses according to the conditions in the fluid being entrained. Typical fluctuating velocity levels would be in the range $10^{-2} < k^{1/2}/U_\infty < 5\times 10^{-2}$, where U_∞ is the freestream velocity. A level of $k^{1/2}/U_\infty$ as low as 1% will normally have no discernible effect on the flow developments within the computation domain. As a word of warning, I have often been assured by students and others unable to make sense of their predictions that they had assigned a very low turbulence intensity level (of about 1%) to the entrained stream. On checking the input file, however, it has emerged that k/U_∞^2 was set to 10^{-2}

* $\tilde{\mu}_{ij}$ is *not* a tensor.

rather than its square root. Thus turbulence energies 100 times stronger than intended were entering. Unless other information is available, it might be supposed that the entrained fluid has an isotropic stress field, i.e. $\overline{u_i u_j} = \frac{2}{3}\delta_{ij}k$. For 'stagnant' surroundings the stresses should differ from zero only by the small amount needed to prevent overflow/underflow in the statements in which they appear.

Prescribed inflow condition. Ignorance of the flow conditions in the inlet stream can cause great uncertainties in the predicted flow pattern. For example, one's interest may be in the flow and surface heat transfer arising from the oblique impingement of a cold jet onto a plane hot surface. One would like to place one boundary of the domain at the exit plane of the jet. However, the surface heat transfer may be much affected by the turbulence at discharge from the pipe, which in turn depends on the pipe length, its surface texture, whether the pipe is curved or straight, etc. The only advice in these cases is to take what guidance one can from experimental data of similar flows and make trial computations to ascertain the effect of varying the inlet values of turbulence quantities by, say, 50%. If the variations in the solutions that result are unacceptably large, the only recourse is to extend the solution domain sufficiently far to make the features of interest less sensitive to the prescribed inlet conditions; for the oblique jet example this would mean extending the calculations into the pipe itself or performing a separate set of calculations of the flow within the pipe.

Outflow conditions. In most flows the prescription of a zero gradient in the direction of the outflowing stream is satisfactory.

Wall boundaries. The no-slip condition at a wall ensures that the turbulent stresses vanish there. Consequently, within a thin sublayer, viscous transport is of considerable importance. To predict the detailed behaviour within this viscosity-affected sublayer requires that the turbulence model should appropriately reflect these viscous influences on the transport processes. Although several groups are working on the development of such models at present, no entirely satisfactory scheme is available even for a flow as uncomplicated as fully developed pipe flow. In making industrial-type computations of wall-bounded flows, therefore, one of two approaches is adopted at present. Either one employs 'wall functions', which provide expressions for the effective overall conductances of the near-wall sublayer,[30,31] or one adopts a simpler model of turbulence within this region. In the examples presented in the next section, comments on the particular near-wall treatment adopted will be made as each example is considered.

SOME ILLUSTRATIVE APPLICATIONS OF SECOND-MOMENT CLOSURES

The examples selected are drawn from those generated by UMIST's CFD research group. This choice is made to allow a selection of examples with identical forms of turbulence model. A complementary set of examples has recently been reported by Leschziner.[28] Efforts in the same direction are underway at a number of research centres around the world. In the U.K. similar types of computation are being made by Dr. W. P. Jones and Dr. J. J. McGuirk at Imperial College[33,34] and Professor Swithenbank's group at Sheffield, in Germany by Professor W. Rodi at the University of Karlsruhe, while in France, particularly in connection with aerodynamic phenomena, the efforts of Professor H. Ha Minh, Dr. D. VanDromme, Dr. J. Delery and Dr. J. Cousteix should be mentioned. In the U.S.A. the application of second-moment closures to industrial flows is probably most advanced in industry itself, with, *inter alia*, GM and GE both

mounting strong efforts, while Creare Inc. have produced the commercial code FLUENT which contains an ASM model of turbulence.

In many of the examples considered below, numerical solutions have been obtained both with a second-moment closure and with a k–ε eddy viscosity model and in these cases results from the two methods are compared.

Confined separated flows

Two examples are chosen here from the many different flows examined in the Ph.D. programmes of Kadja[35] and Yap.[36] The first flow considered is the shear layer arising from the abrupt reduction in diameter of a centre-body mounted in an axisymmetric diffuser (Figure 4). This configuration has been examined experimentally by Lea.[37] The effect of the adverse pressure gradient on the shear flow can be adjusted by moving the centre-body relative to the diffuser section. Kadja's computations of this flow were made on a 44 (streamwise) × 36 (radial) mesh for both an algebraic second-moment closure and the standard k–ε eddy viscosity model with a standard wall function practice used in each case for the near-wall boundary condition. Moreover, for each turbulence model, two practices for discretizing convective transport were adopted: the non-diffusive QUICK scheme of Leonard[38] and Patankar's[39] variant of upwind differencing, PLDS. It is seen from Figure 5(a) that while there is some effect of the discretization scheme (our experience over the past six years leads us unequivocally to prefer the QUICK results[40,41]), a larger factor on the reattachment point is the choice of turbulence model. While both models give reattachment lengths somewhat less than the measurements—a feature common to all the various back-step configurations examined in Reference 35—the ASM results do considerably better. The effect that the different predicted reattachment points have on the static pressure rise on the diffuser wall is shown in Figure 5(b). For both positions of the centre-body the ASM calculations achieve an appreciably better account of the variation of pressure coefficient along the diffuser wall.

Heat transfer coefficients in separated regions are generally much higher than in attached shear flows, a feature that is often exploited in situations where high heat fluxes are required. The actual level of heat transfer coefficient is greatly dependent upon the model of turbulence in the immediate vicinity of the wall and Yap[36] discovered he was unable to achieve satisfactory agreement with a wall function treatment. Instead, a version of the low-Reynolds-number k–ε eddy viscosity model[42,43] was used to span the near-wall sublayer, being merged either to an ASM or an EVM scheme at a short distance from the wall where viscous effects were negligible. In these calculations the turbulent heat fluxes were obtained either by assuming a turbulent thermal eddy

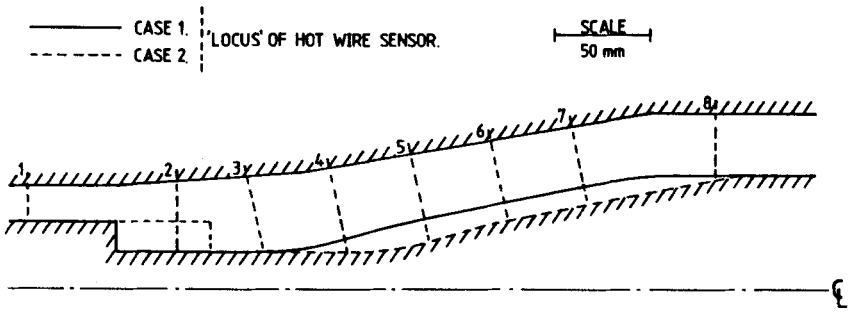

Figure 4. Apparatus for study of separated shear layer developing in conical diffuser

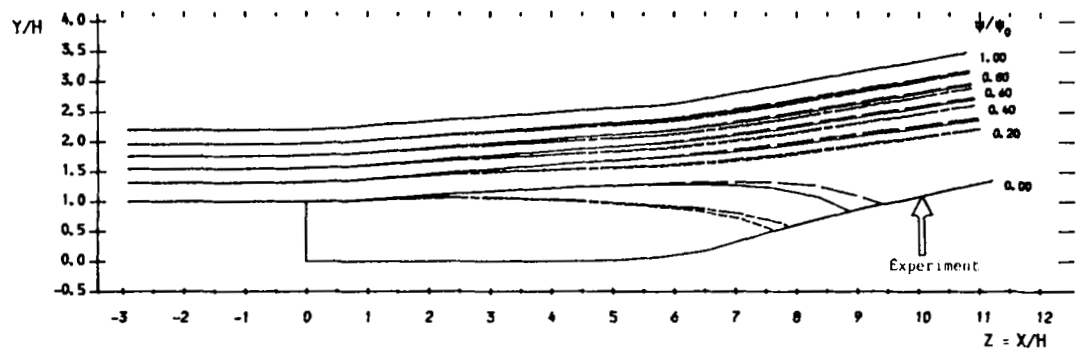

(a)

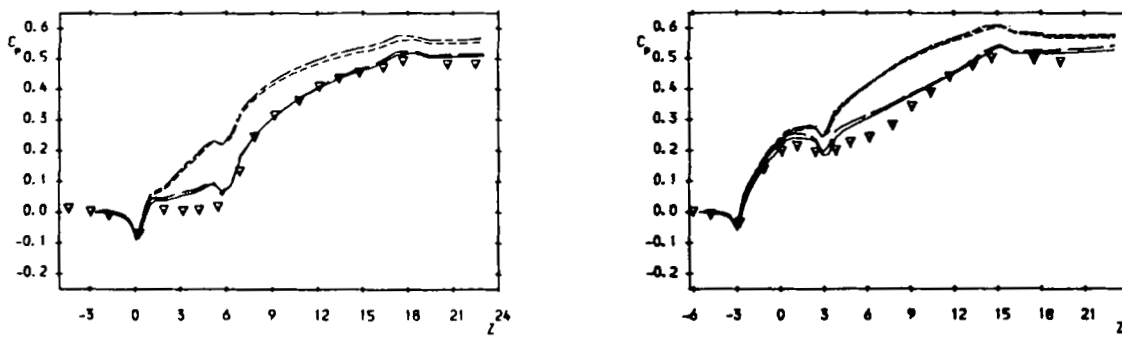

(b)

Figure 5. Comparison of computed and measured development of separated shear layer in axisymmetric conical diffuser: – – –, PLDS (EVM); —·—, QUICK (EVM); ——, PLDS (ASM); — —, QUICK (ASM);[35] ∇, experiment.[37] (a) Computed streamline pattern. (b) Pressure distribution along diffuser wall for two cases

diffusivity of 1/0·9 times the turbulent kinematic viscosity (i.e. a turbulent Prandtl number of 0·9) or, for the ASM calculations, by again invoking the generalized gradient diffusion hypothesis

$$\overline{u_i\theta} = -c_\theta \frac{k}{\varepsilon} \overline{u_i u_k} \frac{\partial \Theta}{\partial x_k}, \tag{16}$$

where θ and Θ refer to fluctuating and mean temperatures and the diffusion coefficient c_θ takes the value 0·3. Figure 6 shows for two Reynolds numbers the resultant profile of Nusselt number downstream of an abrupt 2:1 enlargement in pipe diameter. The flow in the small pipe was fully developed and unheated, while the wall temperature in the larger pipe was maintained at a uniform temperature some 10 °C above that of the entering stream.[44] Measurements suggest that the peak level of Nusselt number occurs at the reattachment point and, as is seen from the figure, actual levels are four to five times greater than the fully developed value that would be reached far downstream. The ASM computations reproduce significantly better than the EVM computations the shape of the Nusselt number curve, including the dependence of the maximum on the Reynolds number; they also give the location of maximum heat flux as occurring at the reattachment point, whereas with the EVM the latter is more than one step height downstream of the former.

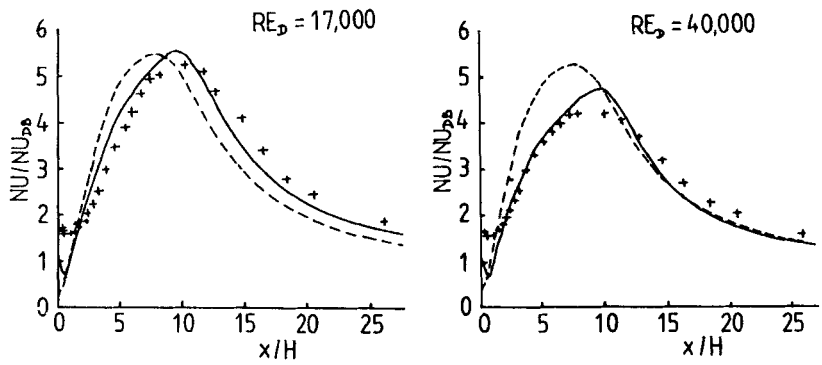

Figure 6. Variation of Nusselt number downstream from an abrupt 2:1 enlargement in pipe diameter: +, measurements;[44] ——, ASM; – – –, EVM[36]

Swirling flows

Swirling flows provide an important and challenging class of axisymmetric shear flows. The performance of swirl combustors and cyclone separators depends crucially on the turbulent flow interactions taking place within them. Here the flow considered is the swirling axisymmetric jet in stagnant surroundings measured by Sislian and Cusworth[45] by laser–Doppler anemometry. The swirl level at discharge was high enough to cause an extensive region of flow recirculation near the axis extending into the discharge pipe itself. Computations reported here were obtained from a full differential stress closure[46] since, as noted in the previous section, the ASM concept fails badly in strongly swirling flows. Figure 7 compares the measured development of the axial and swirl velocity profiles at four stations downstream of the discharge. The standard isotropization of production model (IPS) leads to appreciably too little mixing so the recirculating region on the axis persists too far downstream while the swirl velocity decays too slowly. The modified coefficients proposed by Younis[14] ($c_1 = 3{\cdot}0$, $c_2 = {\cdot}3$) bring some improvement but the closest agreement results from IPC, the convection-modified version, equation (10).

Flows through rotating ducts

The field of turbomachinery provides many practical examples of turbulent flow through rotating passages. In this class of flows one finds important contributions from Coriolis forces that affect both the mean flow and the turbulent stresses. Experimentally it is usually hard to separate these two contributions. For one case, however—that of fully developed flow between (effectively) infinite rotating parallel planes—the Coriolis forces on the mean flow are exactly balanced by static pressure gradients. Thus any differences in the flow pattern from that of the corresponding non-rotating flow are unequivocally due to effects of Coriolis forces on the turbulence. If we rotate our co-ordinate frame, an effective source F_{ij} enters the Reynolds stress transport equation given by

$$F_{ij} = -2\rho\Omega_k(\overline{u_j u_m}\,\varepsilon_{ikm} + \overline{u_i u_m}\,\varepsilon_{jkm}), \tag{17}$$

where Ω_k is the co-ordinate rotation vector and ε_{ikm} the third-rank alternating tensor. Thus, for the co-ordinate system shown in Figure 8, a term $-4\Omega\overline{uv}$ appears in the $\overline{v^2}$ equation while the same term with opposite sign is present in the $\overline{u^2}$ equation. Now, in the adopted co-ordinates, the shear stress $\overline{uv}$ will be negative near the pressure surface and positive near the 'suction' surface. Thus we

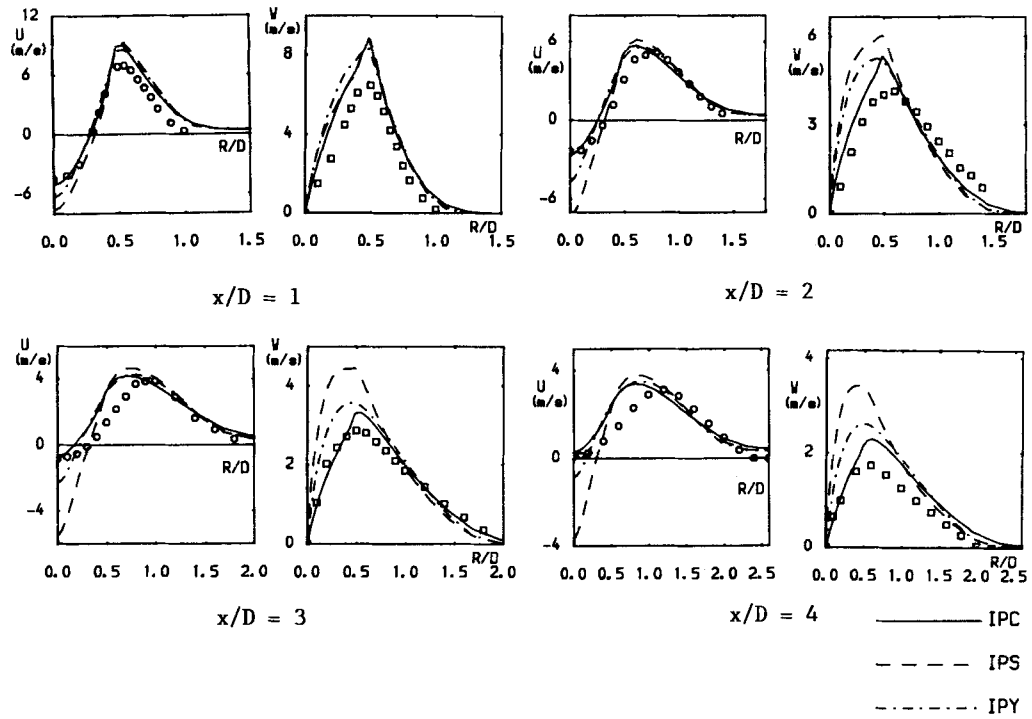

Figure 7. Development of axial and swirl components of mean velocity: □, ○, measurements;[45] —— computations[46]

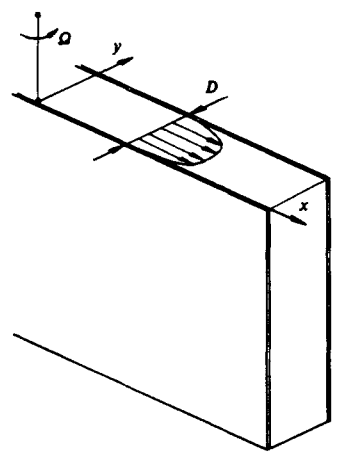

Figure 8. Co-ordinate frame for rotating duct

should expect that $\overline{v^2}$, the fluctuating component primarily responsible for turbulent mixing, will be increased near the pressure surface and decreased near the suction. Figure 9 compares the predicted profile of this quantity[47] obtained from a full second-moment closure (using wall functions) with that found from the large-eddy simulation of Kim:[48] the departures from the non-rotating case are evidently well captured by the second-moment closure. The modification of the

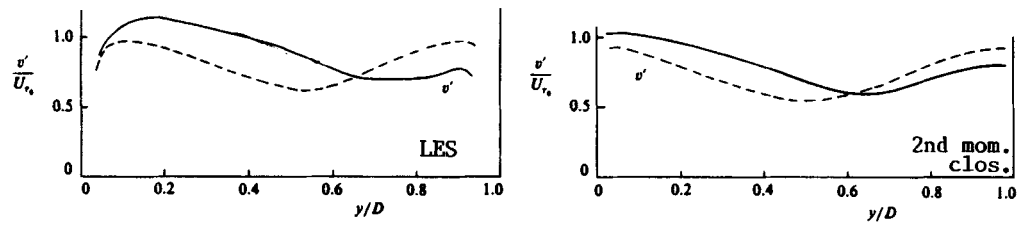

Figure 9(a). Comparison of $\overline{v^2}$ distributions in stationary and rotating channels for second-moment closure and large-eddy simulation

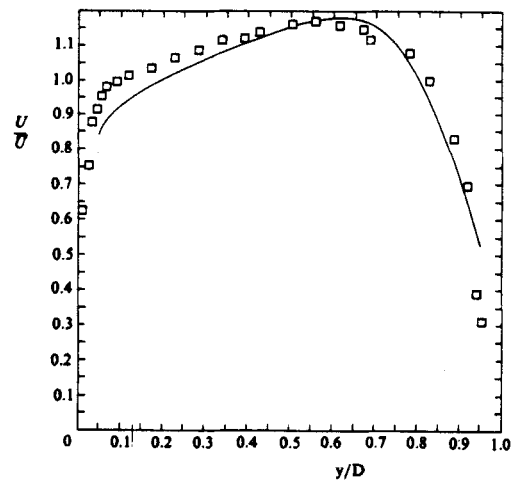

Figure 9(b). Mean velocity profile for rotation number = 0·21:——, Launder *et al.*;[47] □, Johnston *et al.*[49]

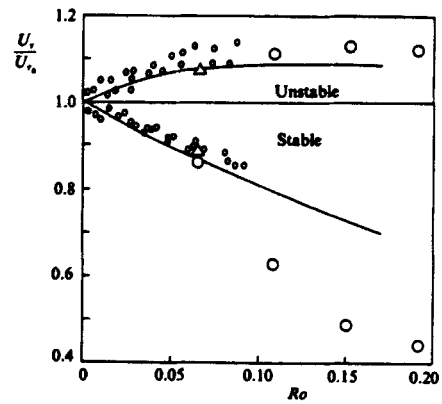

Figure 9(c). Skin friction dependence on rotation number: ——, computations;[47] ○, experiments;[49] Δ, LES[48]

Reynolds stress field in turn produces a strongly asymmetric distribution of mean velocity and a corresponding effect on the wall shear stress. Again the changes are broadly in line with the available measurements.[49] As a footnote, we remark that had the standard k–ε eddy viscosity model been used to compute this flow, an entirely symmetric pattern would have resulted since the turbulence energy generation rate is entirely unaffected by rotation.

In practical situations, channels are of finite extent in the direction of the rotation axis and thus secondary flows are induced. Figure 10, for example, shows the computed secondary flow pattern and axial velocity contours obtained[50] for flow in a circular pipe in orthogonal mode rotation for a Reynolds number of 25000 and a rotation number of 0·183, levels typical of those found in the internal cooling holes in gas turbine blades. The turbulence model employed was the standard ASM closure, but near the wall, in place of the wall functions adopted in the plane channel study, Van Driest's[51] version of the mixing-length hypothesis was used. This replacement was introduced because, due to the secondary velocity peaking so near the wall, very near the wall the mean velocity vector undergoes a rapid change in direction with distance from the wall, a feature which the coarse-grid wall-function approach is not successful at reproducing. Detailed experimental data are not available for this configuration but Reference 52 has recorded the effect of rotation on the overall streamwise pressure gradient in the tube, thus enabling the mean friction factor c_f to be determined. They found their data were well correlated by the equation

$$c_f/c_{f0} = 0{\cdot}942 + 0{\cdot}058\,(Ro^2\,Re)^{0.282}, \tag{18}$$

which is shown as the solid curve in Figure 10. Here c_{f0} is the friction factor at the same Reynolds number (Re) without rotation and Ro is the rotation number, defined as pipe diameter times

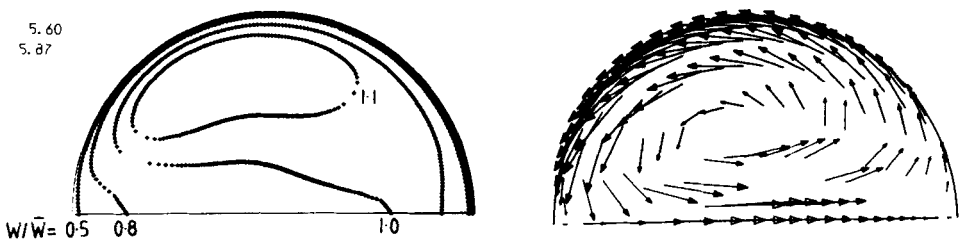

Figure 10(a). Axial velocity contours and secondary flow vectors obtained from ASM computation[50]

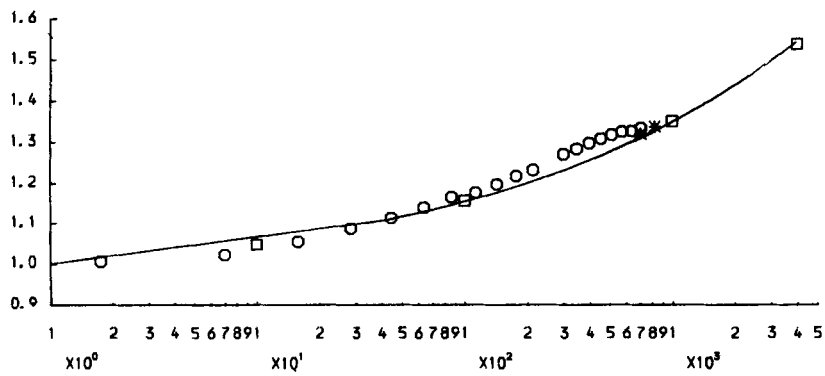

Figure 10(b). Measured and computed effects of rotation on friction factor: ——, equation (18), correlation of experimental data; symbols, computations at two Reynolds numbers

angular velocity divided by bulk mean velocity. Predictions resulting from the ASM computations of Reference 50 are shown by symbols. There is indeed an extremely close correspondence between the two.

Flow around bends

The code developed for flow in rotating straight ducts above can also be applied to bend flows (whether rotating or stationary). This class of flows is the focus of our final comparison. The flow in this case is three-dimensional and, depending on the application, between 100 and 150 streamwise planes have been employed to resolve accurately the streamwise development. From the several test cases examined[29, 53, 54] we consider the flow development around a 180° bend of square cross-section for which Chang *et al.*[55] have reported detailed experimental data. A particularly interesting feature of this flow is that by halfway around the bend axial velocity profiles along lines parallel to the symmetry plane develop double peaks due to the secondary motion. The initial computational studies of this flow,[56] which adopted wall functions and the k–ε EVM, entirely missed this feature. We have therefore repeated the computations, replacing the wall functions by a fine near-wall grid in which the mixing-length hypothesis was employed. In the core region results have been obtained with both the standard k–ε EVM and ASM treatments. Streamwise velocity profiles obtained in Reference 54 at a position 130° from entry to the bend are shown in Figure 11. The inclusion of a fine-grid/mixing-length treatment over the sublayer itself brings a considerable improvement in the realism of the prediction compared with that obtained in Reference 56: significant double maxima in velocity now appear in the computations. The calculated behaviour obtained with an ASM treatment, however, is in significantly closer accord

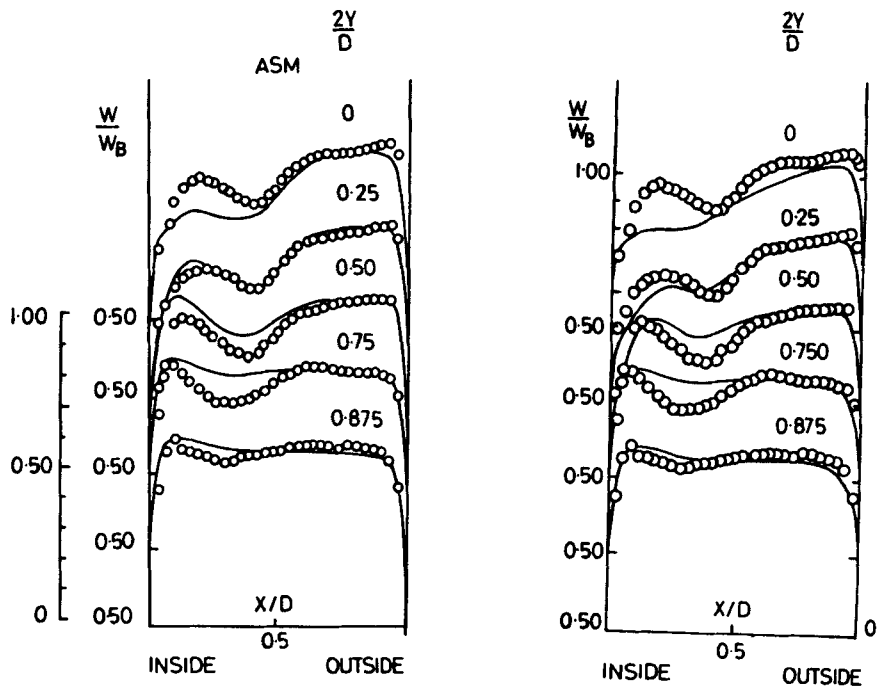

Figure 11. Streamwise velocity profiles at 130° station in square-sectioned U-bend. Comparison of ASM and EVM performance: ○, experiments;[56] ——, computations[55] (left curves are ASM results)

with the reported experimental data. In fact the streamwise velocity profiles are to a large extent shaped by the secondary flow pattern and we note in Figure 12 a considerable difference between the secondary flow vectors for the two models. The relative weakness of the viscous-type linkages with neighbouring nodes associated with the ASM treatment makes it easier for the flow to break up into multiple secondary eddies than with an eddy viscosity model. As we see in Figure 12, not only is an additional eddy present with the former scheme but the secondary eddies are also rather more distinct. Although direct experimental data are not available, there seems little doubt that the pattern predicted with the ASM is closer to the actual flow.

PROSPECTS

The previous section has presented a sample of the complex shear flows computed in the last 18 months at UMIST. While the writer would admit to having biased his selection slightly in favour of flows showing the better agreement with experiment, the relative performance of the second-moment and eddy viscosity schemes suggested by the comparisons is a balanced one. Sometimes an eddy-viscosity-based computation gives an entirely satisfactory result; and sometimes a second-moment closure prediction seriously fails to mimic the real flow; but hardly ever does the standard second-moment closure give a worse result than the standard k–ε eddy viscosity model. Thus a changeover from the latter model (where most of today's industrial flow calculations are performed) to the former offers the assured prospect of greater predictive realism.

Yet, given that computations with a Reynolds-stress-based turbulence model will probably require between 50% and 150% more computer time than a two-equation eddy viscosity model, can their accuracy not be improved still further to give greater justification for the added expense? The great amount of effort directed at fundamental model improvement rather than application suggests that the modelling community believes the answer to be affirmative. In closing, therefore, a few paragraphs are devoted to giving the flavour of this research.

In the second section both the turbulence and the mean-strain part of ϕ_{ij} were modelled by forms linear in the Reynolds stress. However, the exact integral for ϕ_{ij1} (see equation (7)) explicitly suggests a *non*-linear form. We might also expect some non-linear effect in ϕ_{ij2} since the isocorrelation surfaces of the two-point velocity products will themselves be distorted by the anisotropy of the stress field. Various non-linear forms have been suggested for both processes. A generalized form for the turbulence part may be written

$$\phi_{ij1} = -c_1 \varepsilon [a_{ij} + \alpha(a_{ik}a_{kj} - \tfrac{1}{3}\delta_{ij}A_2)], \tag{19}$$

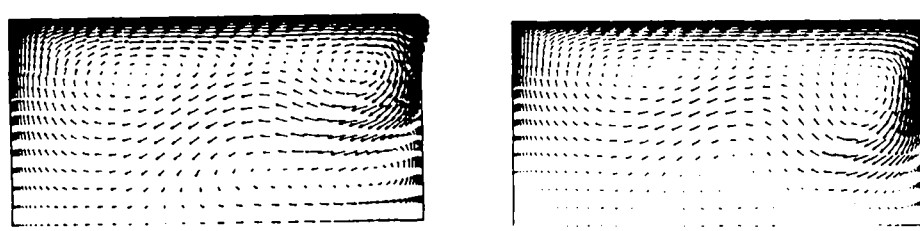

a) b)

Figure 12. Comparison of computed secondary flow vectors: (a) EVM; (b) ASM[55]

where A_2 is the second invariant $a_{ik}a_{ki}$ and c_1 and α are prescribed constants or functions of the stress invariants. These coefficients are determined partly by fitting experimental data and partly by applying formal constraints, for example by requiring that $\phi_{\beta\beta}$ should vanish if $\overline{u_\beta u_\beta}$ becomes zero. Most approaches to date[12,57] have taken $\alpha = 0$, thus incorporating all the non-linearity in the dependence on c_1 on A_2 and A_3 ($\equiv a_{ik}a_{kj}a_{ji}$). As Lumley[12] has shown, the two-dimensional limit can be accommodated by noting that in this case the quantity $A \equiv 1 - \frac{9}{8}(A_2 - A_3)$ vanishes identically. Thus a relationship of the form $c_1 = c_1(A)$ will give the desired limit. However, our recent experience at UMIST suggests that, to capture adequately the non-linear characteristics of ϕ_{ij1}, the quantity α in (19) must also be non-zero.[58]

Shih and Lumley[57] have devised a quadratic form for ϕ_{ij2} which, *inter alia*, also satisfies the two-dimensional limit. It may be written

$$\begin{aligned}\phi_{ij2} = & -(0{\cdot}6 + \tfrac{4}{75}A^{1/2})(P_{ij} - \tfrac{1}{3}\delta_{ij}P_{kk}) - \tfrac{32}{75}A^{1/2}(D_{ij} - \tfrac{1}{3}\delta_{ij}D_{kk}) \\ & - \tfrac{16}{50}A^{1/2}k\left(\frac{\partial U_i}{\partial x_j} + \frac{\partial U_j}{\partial x_i}\right) + 0{\cdot}3\,a_{ij}P_{kk} \\ & - 0{\cdot}2\left[\frac{\overline{u_k u_j}\,\overline{u_l u_j}}{k}\left(\frac{\partial U_k}{\partial x_l} + \frac{\partial U_l}{\partial x_k}\right) - \frac{\overline{u_i u_k}}{k}\left(\overline{u_i u_k}\frac{\partial U_j}{\partial x_l} + \overline{u_j u_k}\frac{\partial U_i}{\partial x_l}\right)\right]. \end{aligned} \tag{20}$$

Following a similar approach at UMIST,[58] we have arrived at

$$\begin{aligned}\phi_{ij2} = & -0{\cdot}6(P_{ij} - \tfrac{1}{3}\delta_{ij}P_{kk}) + 0{\cdot}3\,a_{ij}P_{kk} \\ & - 0.2\left[\frac{\overline{u_k u_j}\,\overline{u_l u_j}}{k}\left(\frac{\partial U_k}{\partial x_k} + \frac{\partial U_l}{\partial x_k}\right) - \frac{\overline{u_i u_k}}{k}\left(\overline{u_i u_k}\frac{\partial U_j}{\partial x_l} + \overline{u_j u_k}\frac{\partial U_i}{\partial x_l}\right)\right] \\ & - r\,[A_2(P_{ij} - D_{ij}) + 3\,a_{mi}\,a_{nj}(P_{mn} - D_{mn})], \end{aligned} \tag{21}$$

which with $r = 0{\cdot}7$ has been applied successfully in a number of homogeneous shear flows. The model has also been applied with interesting effect by Fu *et al.*[46] in computing the swirling jet considered earlier. Although in this case the overall spread and decay were not particularly well captured, some features in the computed stress field, which in the earlier computations had been missed, were now correctly reproduced. The authors concluded that weaknesses in computing the energy dissipation rate were probably responsible for much of the remaining discrepancy between experiment and computation.

Indeed, throughout the history of second-moment closures, the determination of ε (or equivalently of a typical length or time scale of the energy-containing eddies) has been the weakest point in the model. The problem is the absence of a directly useful exact equation to serve as a framework for modelling. Numerous amendments to the standard form, equation (6), have been proposed, mainly to modify the generation process. These include:

(1) the inclusion of an additional source term involving the mean vorticity[59,60]
(2) the introduction of a source of the form $f(A_2)\varepsilon^2/k$ as a partial replacement for mean-strain contributions[12,61]
(3) the addition of a term proportional to *gradients* in the energy dissipation and energy to prevent excessive length scales developing in separated near-wall regions.[36,62]

In truth, one probably needs to include *all* the above influences to achieve the greatest width of applicability. While such an optimized form is probably still some way off, it seems that any one of a number of proposals is likely to bring a modest improvement over equation (6).

Finally, a few remarks are in order about second-moment closures for the near-wall 'buffer' region—'low-Reynolds-number' models as they are sometimes called. With the very simplest turbulence model—the mixing-length hypothesis—one has to reduce the mixing length in the buffer region to prevent excessive turbulent transport rates there. To this end, Van Driest's damping function[51] is commonly employed with the 'universal' co-ordinate $y^+ \equiv \rho y \sqrt{(\tau_w/\rho)}/\mu$ as the argument. In higher-order eddy viscosity models one also damps the turbulent viscosity by a function proportional to a local turbulent Reynolds number, $\rho k^2/\mu\varepsilon$ say. When the modelling level was extended to second-moment closures, the same tactic was employed to bring about a transition from predominantly viscous to predominantly turbulent transport over the correct range of y^+. Yet, in fact, most of the 'damping' of the turbulent stress as the wall is approached is due not to viscous action but to the precipitate decline of $\overline{v^2}$, which in turn results from the cutting off of the energy supplied to it via ϕ_{ij}. Thus to model properly the dynamics of the buffer region, it is very important to adopt models of ϕ_{ij} that satisfy the two-dimensional constraint discussed above. Work in progress at UMIST suggests that, with a proper respect for this limit, the need for genuinely viscous damping virtually disappears and, moreover, the strength of the wall echo ϕ_{ij}^w can be considerably reduced. Since the prospect of developing a general model of the wall echo process on highly non-planar surfaces is remote, this discovery is encouraging.

Many of the most important applied problems in turbulence modelling in the next decade centre around the intelligent control and modification of this sublayer region, whether it be to enhance (or inhibit) heat transfer, prevent separation or reduce drag. While it is unlikely that riblets won the Americas Cup for the Americans in 1987, perhaps creative, applied CFD, incorporating buffer layer turbulence modelling, will help the Aussies regain it in 1991!

ACKNOWLEDGEMENTS

Sincere thanks go to my academic colleagues Dr. M. A. Leschziner and Dr. H. Iacovides who have made major contributions to the development of the software used to generate the computations reported in this paper. Different aspects of the research have been supported by the SERC, Rolls-Royce plc and the Ministry of Defence Procurement Executive. Production of the manuscript has been handled with skill and care by Mrs. L. J. Ball.

REFERENCES

1. W. P. Jones and B. E. Launder, *Int. J. Heat Mass Transfer*, **15**, 301 (1972).
2. J. C. Rotta, *Z. Phys.*, **129**, 547 (1951).
3. C. du P. Donaldson, *AIAA J.*, **7**, 271 (1969).
4. B. J. Daly and F. H. Harlow, *Phys. Fluids*, **13**, 2634 (1970).
5. K. Hanjalic and B. E. Launder, *J. Fluid Mech.*, **52**, 609 (1972).
6. H. P. A. H. Irwin and P. Arnot-Smith, *Phys. Fluids*, **18**, 264 (1975).
7. S. B. Pope and J. H. Whitelaw, *J. Fluid Mech.*, **73**, 9 (1976).
8. P. A. Libby, 'Studies in variable density and reacting shear flows', in B. E. Launder (ed.), *Studies in Convection—2*, Academic Press, London, 1977.
9. P. Bradshaw, '*Turbulence*', in *Topics in Applied Physics, Vol. 12*, Springer, Heidelberg, 1976, Ch. 6.
10. B. I. Davidov, *Dokl. Akad. Nauk. SSSR*, **136**, 47 (1961).
11. P.-Y. Chou, *Q. Appl. Math.*, **3**, 31 (1945).
12. J. L. Lumley, *Adv. Appl. Mech.*, **18**, 123 (1978).
13. D. Naot, A. Shavit and M. Wolfshtein, *Israel J. Technol.*, **8**, 259 (1970).
14. B. A. Younis, *Ph.D. thesis*, Faculty of Engineering, University of London, 1970.
15. M. M. Gibson and B. A. Younis, *Phys. Fluids*, **29**, 36 (1986).
16. B. E. Launder, A. P. Morse, W. Rodi and D. B. Spalding, *Proc. 1972 Langley Free Shear Flows Conf.; NASA SP 320*, 1973.
17. D. Naot, A. Shavit and M. Wolfshtein, *Phys. Fluids*, **16**, 738 (1973).

18. B. E. Launder, G. Reece and W. Rodi, *J. Fluid Mech.*, **68**, 537 (1975).
19. J. L. Lumley, 'Prediction methods for turbulent flow—introduction', *Lecture Series 76*, Von Karman Institute, 1975.
20. B. E. Launder, W. C. Reynolds and W. Rodi, *Turbulence Models and Their Applications*, Eyrolles, Paris, 1984.
21. B. E. Launder and A. Morse, 'Numerical prediction of axisymmetric free shear flows with a second-order Reynolds-stress closure', *Turbulent Shear Flows—1*, Springer, Heidelberg, 1979.
22. D. Naot and W. Rodi, *J. Hydraul. Div. ASCE*, **108**, 948 (1982).
23. M. M. Gibson and B. E. Launder, *J. Fluid Mech.*, **86**, 491 (1978).
24. W. Rodi, *ZAMM*, **56**, 219 (1975).
25. B. E. Launder, *AIAA J.*, **20**, 436 (1982).
26. S. Fu, P. G. Huang, B. E. Launder and M. A. Leschziner, *J. Fluids Eng.*, **110**, 216 (1988).
27. P. G. Huang and M. Leschziner, 'Stabilization of recirculating flow computations performed with second-order closures and third-order discretization', *Proc. 5th Symp. on Turbulent Shear Flows*, Cornell University, 1985, Paper 20.7.
28. M. A. Leschziner, 'Numerical implementation and performance of Reynolds-stress closures in finite-volume computations of recirculating,and strongly swirling flows', *Notes for 'An Introduction to the Modelling of Turbulence'; VKI Lecture Series 1987–06*, 1987.
29. H. Iacovides and B. E. Launder, *Proc. 4th Int. Conf. on Numerical Methods in Laminar and Turbulent Flows*, Pineridge Press, Swansea, 1985, pp. 1023–1045.
30. W. Kebede, B. E. Launder and B. A. Younis, 'Large-amplitude periodic flows: a second-moment-closure study', *Proc. 5th Symp. on Turbulent Shear Flows*, Cornell University, 1985, Paper 16.23.
31. B. E. Launder and D. B. Spalding, *Comput. Methods Appl. Mech. Eng.*, **3**, 269 (1974).
32. C. C. Chieng and B. E. Launder, *Numer. Heat Transfer*, **3**, 189 (1980).
33. J. J. McGuirk and H. Papadimitriou, 'Buoyant surface layers under fully entraining and internal hydraulic jump conditions', *Proc. 5th Symp. on Turbulent Shear Flows*, Cornell University, 1985, Paper 22.13.
34. W. P. Jones and A. J. Marquis, 'Calculation of axisymmetric recirculating flows with a second-order turbulence model', *Proc. 5th Symp. on Turbulent Shear Flows*, Cornell University, 1985, Paper 20.1.
35. M. Kadja, 'Computation of recirculating flow in complex domains with algebraic Reynolds stress closure and body-fitted meshes', *Ph.D. thesis*, Faculty of Technology, University of Manchester, 1987.
36. C. R. Yap, 'Turbulent heat and momentum transfer in recirculating and impinging flows', *Ph.D. thesis*, Faculty of Technology, University of Manchester, 1987.
37. C. J. Lea, 'Hot-wire measurements of turbulent flow over a sudden centrebody contraction placed in a diffuser', *M.Sc. thesis*, Faculty of Technology, University of Manchester, 1987.
38. B. P. Leonard, *Comput. Methods Appl. Mech. Eng.*, **19**, 59 (1979).
39. S. V. Patankar, *Numerical Heat Transfer and Fluid Flow*, McGraw Hill/Hemisphere, New York, 1980.
40. T.-Y. Han, J. A. C. Humphrey and B. E. Launder, *Comput. Methods Appl. Mech. Eng.*, **29**, 81 (1981).
41. P. G. Huang, B. E. Launder and M. A. Leschziner, *Comput. Methods Appl. Mech. Eng.*, **48**, 1–24 (1985).
42. W. P. Jones and B. E. Launder, *Int. J. Heat Mass Transfer*, **16**, 1189 (1973).
43. B. E. Launder and B. I. Sharma, *Lett. Heat Mass Transfer*, **1**, 131 (1974).
44. J. W. Baughn, M. A. Hoffman and D.-H. Lee, 'Heat transfer measurements downstream of an abrupt pipe expansion in a circular duct with constant wall temperatures', *ASME Winter Annual Meeting*, Anaheim, 1986, Paper 86-WA/HT-100.
45. J. P. Sislian and R. A. Cusworth, 'Laser–Doppler velocimetry measurements in a free isothermal swirling jet', *Report 281, CN ISSN 0082-5255*, University of Toronto Institute of Applied Science, 1984.
46. S. Fu, B. E. Launder and M. A. Leschziner, 'Modelling strongly swirling recirculating jet flow with Reynolds-stress transport closures', *Proc. 6th Symp. on Turbulent Shear Flows*, Toulouse, 1987, Paper 17-6.
47. B. E. Launder, D. P. Tselepidakis and B. A. Younis, 'A second-moment closure study of rotating channel flow', *J. Fluid Mech.*, **183**, 63 (1988).
48. J. Kim, *Proc. 4th Symp. on Turbulent Shear Flows*, University of Karlsruhe, 1983, Paper 6.14.
49. J. P. Johnston, R. M. Halleen and D. K. Lezius, *J. Fluid Mech.*, **56**, 533 (1972).
50. H. Iacovides and B. E. Launder, 'Numerical simulation of flow and heat transfer in tubes in orthogonal-mode rotation', *Proc. 6th Symp. on Turbulent Shear Flows*, Toulouse, 1987, Paper 1-5.
51. E. R. Van Driest, *J. Aero. Sci.*, **23**, 1007 (1956).
52. H. Ito and K. Nanbu, *ASME J. Basic Eng.*, **93**, 383 (1971).
53. H. Iacovides, B. E. Launder and P. A. Loizou, 'Numerical computation of turbulent flow through a square-sectioned 90° bend', *Int. J. Heat Fluid Flow*, **8**, 320 (1988).
54. Y.-D. Choi, H. Iacovides and B. E. Launder, 'Numerical computation of turbulent flow in a square-sectioned 180° bend', *J. Fluids Eng.* to appear (1988).
55. S. M. Chang, J. A. C. Humphrey and A. Modavi, *Phys. Chem. Hydrodyn.* **4**, 243 (1983).
56. R. W. Johnson, 'Turbulent convecting flow in a square duct with a 180° bend: an experimental and numerical study', *Ph.D. thesis*, Faculty of Technology, University of Manchester, 1984.
57. T.-H. Shih and J. L. Lumley, 'Modeling of pressure correlation terms in Reynolds stress and scalar flux equations', *Report FDA-85-3*, Sibley School of Mechanical and Aerospace Engineering, Cornell University, 1985.
58. S. Fu, B. E. Launder and D. P. Tselepidakis, 'Accommodating the effects of high strain rates in modelling the pressure–strain correlation', Report TFD/87/5, Mech. Eng. Dept, UMIST, 1987.

59. S. B. Pope, *AIAA J.*, **16,** 279 (1978).
60. K. Hanjalic and B. E. Launder, *ASME J. Fluids Eng.*, **102,** 34 (1980).
61. O. Zeman and J. L. Lumley, *Turbulent Shear Flows—1*, Springer, Heidelberg, 1979.
62. D. Wilcox and M. W. Rubesin, 'Progress in turbulence modelling for complex flow fields including effects of compressibility', *NASA Technical Paper 1517*, NASA Ames Research Center, 1980.